



# Understanding Karst Conduit Size Distribution by Numerical Speleogenesis Modeling

A. Maqueda, P. Renard, and M. Filipponi

## Abstract

Large karstic conduits are rare within a rock formation, and therefore, the probability of encountering them during the construction of a tunnel is relatively low. However, the consequences can be dramatic for tunnel worker safety and/or the economic aspects of the tunnel realization, therefore, the risk must be accounted for. One of the critical aspects when evaluating the karst-related hazards is to estimate the statistics of the size of the conduits, as well as the connectivity of the karst network. This information is fundamental for a reliable risk assessment. Statistical analysis can be carried out from data collected by speleologists, but a large portion of the karst conduit network is not directly accessible, and therefore, the resulting statistics are incomplete. An alternative to assess the inaccessible areas of a karst conduit network is the use of numerical simulations of the speleogenesis processes. The premise is that the numerical simulation of groundwater flow on a connected fracture network, including mineral dissolution, will produce a conduit network that shares properties of real networks. We simulated the enlargement of fracture networks and conducted a statistical analysis of the results to obtain possible statistical distributions of conduit sizes and spatial distribution of the conduit network. These findings will better constrain hazards concerning the construction of tunnels. Furthermore, our results confirm numerically a conceptual model of staged cave development previously introduced.

A. Maqueda (✉)

AFRY Schweiz AG, Herostrasse 12, CH-8048 Zürich, Switzerland  
e-mail: [axayacatl.maqueda@afry.com](mailto:axayacatl.maqueda@afry.com)

P. Renard

Centre d'hydrogéologie (CHYN), Rue Emile-Argand 11, CH-2000 Neuchâtel, Switzerland

M. Filipponi

National Cooperative for Disposal of Radioactive Waste (Nagra), Hardstrasse 73, CH-5430 Wettingen, Switzerland

## Keywords

Karst • Mineral dissolution • Speleogenesis • Conduit statistics

## 1 Introduction

Karst aquifers develop when carbonate rocks are locally dissolved by groundwater. The global behavior of these aquifers is dominated by fast groundwater flow within the karst conduits. When tunnels are constructed in such environments, they face the risk of encountering a conduit, and when these accidents occur, the consequences can be dramatic because the tunnel can rapidly be flooded. Usually, large karst conduits are rare within a rock formation, and therefore, the probability of encountering them is relatively low, but the consequences being potentially very severe the risk must be accounted for. Casagrande et al. (2005), Filipponi et al. (2012) and Jeannin et al. (2015) report several examples of such events and discuss methods to evaluate the risks. One of the critical aspects when evaluating the karst-related hazards is to estimate the statistics of the dimensions of the conduits, as well as the connectivity of the karst network. The work presented in this paper aims to generate possible statistical distributions of the conduit size and spatial distribution of the karst conduit network to better constrain hazards concerning the construction of tunnels. For that purpose, we simulated speleogenesis processes and assessed how the distribution of the conduit size evolves before and after breakthrough flow in fractures.

## 2 Speleogenesis Conceptual Model and Software Development

We developed the FEFLOW 7 plug-in **Karstification Simulation Plug-in (KSP)** to simulate the enlargement of fractures by mineral dissolution. FEFLOW is a finite element software

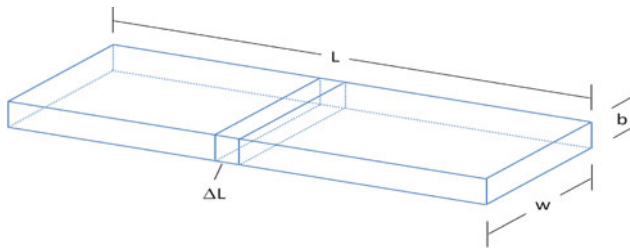


**Fig. 1** Fracture enlargement conceptual model

to simulate groundwater flow and reactive transport in porous and fractured media. The current development is based on the research work and past software development at the University of Neuchâtel (Maqueda 2017). The modeling approach is based on the conceptual model presented by Dreybrodt et al. (2005). The model represents the feedback loop between mineral dissolution and the flow of reactive water through fractures. The model computes the growth of fracture opening due to mineral dissolution and then the flow field is updated. The basic model assumes water with a known solute concentration flows through a planar fracture (Fig. 1).

The conceptual model relies on two assumptions. The first assumption is the fracture walls are assumed to be pure calcite rock ( $\text{CaCO}_3$ ) therefore soluble by reactive water. The second assumption is the dissolution reaction occurs at the rock surface only, and the effect of calcite dissolution is a retreat of the fracture wall. FEFLOW can simulate both laminar and turbulent flow in fractures. KSP accounts in addition for the transition between laminar and turbulent flow and can estimate the wall retreat for both flow regimes. Water flow in fractures is described by the Hagen-Poiseuille equation for laminar flow and Manning–Strickler for turbulent flow. Mass transport is described by the advective-diffusion equation applied to only one dissolved species: calcium ion ( $\text{Ca}^{2+}$ ). The simulation of calcite dissolution is based on the kinetics chemistry model of Dreybrodt et al. (2005) which was developed from laboratory experiments of pure calcite dissolution under laminar and turbulent flow conditions. Mineral dissolution is the only driver of fracture growth with KSP. Other processes known to contribute to the growth of karst conduits in nature are not accounted for: erosion of walls by suspended solids in water, a local increase of water acidity (e.g., pyrite weathering), or rock detachment along the conduit walls due to mechanical stress.

### 3 KSP Benchmark Test

We first applied KSP to replicate a simulation of the enlargement of a single fracture published by Dreybrodt et al. (2005) to test the KSP code. The available data include the results of a numerical simulation and an analytical approximation for the transition from laminar to turbulent

flow. There are two fundamental differences between the original paper and our implementation. In the benchmark, flow occurs only in fractures and hydrodynamic dispersion of mass is not accounted for. In our simulation, fractures are embedded in a porous rock matrix with low hydraulic conductivity ( $<1 \times 10^{-6}$  m/s), where flow and solute transport still occur at a minimal rate, and we use an advective-dispersion transport model that considers hydrodynamic dispersion. Hydrodynamic dispersion accounts for the heterogeneity in water flow velocity in fractures.

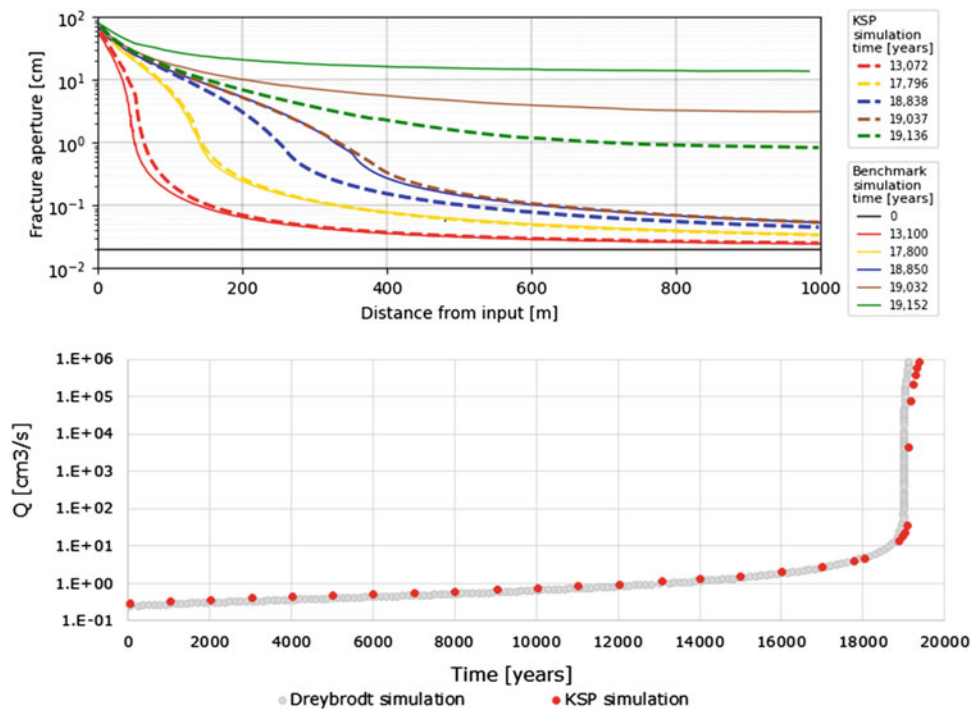
The benchmark model consists of a rectangular fracture having a width of 1 m and an initial aperture of 0.0002 m (0.2 mm) and a length of 1000 m. The hydraulic boundary condition is a constant hydraulic head of 50 m at the inlet point and 0 m at the outlet. The solute boundary condition is water fully unsaturated with calcite at the inlet. The calcite equilibrium concentration is 2 mmol/l. The linear and fourth-order reaction kinetics constant values are  $4 \times 10^{-7}$  and  $4 \times 10^{-4}$ , respectively.

Figure 2 (top) presents the evolution of fracture aperture in both the KSP simulation (dashed lines) and the benchmark (solid lines). At simulation times of 13,100 and 17,800 yrs., the fracture aperture in both simulations is nearly identical. The transition to turbulent flow occurs at 18,850 yrs., and the fracture apertures in the KSP simulation are slightly smaller than the benchmark (blue lines). The greatest difference in fracture aperture is observed at a simulation time of 19,032 yrs. The deviations can be explained by differences due to the presence of porous media in KSP and the different transport equations. At a simulation time of 19,152 yrs., the difference in fracture aperture is reduced after flow becomes turbulent. Figure 2 (bottom) presents the evolution of flow rate for both KSP simulation and benchmark. Simulated flow rates with KSP are very similar before and after the transition to laminar flow (nearly vertical increase in flow rate). Only a small difference is observed by the end of the simulation.

We conclude from this test that KSP reproduces the main trends of fracture aperture and flow rate evolution of the benchmark. In addition, it can model the transition between laminar and turbulent flow. Finally, we consider that this test shows that KSP is capable to simulate reasonably well fracture growth from  $10^{-4}$  m to 10 m. In the next section, we apply KSP to fracture networks.

### 4 Speleogenesis Simulation in Synthetic Fracture Networks

We apply KSP to investigate the evolution of synthetic fracture networks under conditions that we consider closer to aquifers in nature. The groundwater flow rate is limited by precipitation and subsoil recharge in the vadose zone, see the conceptual model in Fig. 3. The top boundary of the model



**Fig. 2** Evolution of fracture aperture and flow rate in Dreybrodt benchmark and KSP simulation

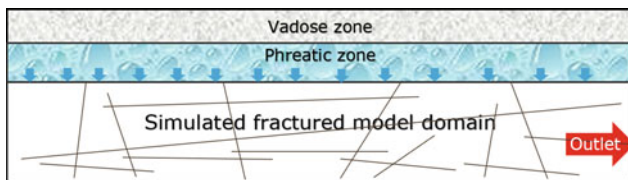


**Fig. 3** Conceptual model of a fracture network under phreatic conditions in a carbonate aquifer

is assumed to be the bottom of a shallow unconfined aquifer. Water inflow is not constant because rainfall is occasional. The vadose zone and an aquifer on top of the model domain act as buffers for intermittent precipitation. The aquifer provides a nearly constant hydraulic head on top of the simulated domain. When fracture apertures are small (mm), the hydraulic gradient is high because small fractures have a great resistance to flow. When fracture apertures grow to the size of karst conduits, groundwater recharge is the limiting factor. Therefore, we assumed a hydraulic boundary condition of high initial constant head and maximum flow rate.

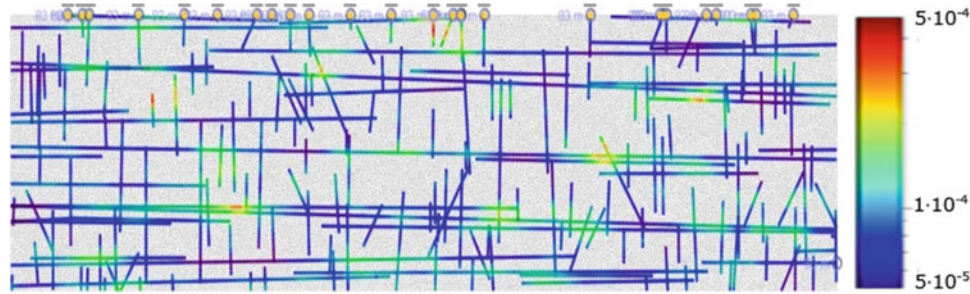
The model domain for a fracture network has a size of 2000 m horizontally and 500 m vertically. The initial fracture network was generated using an object-based model implemented in Python code. We defined 4 families of discontinuities that correspond to a simplified realistic situation where a rock massif is in extension. The horizontal family represents bedding planes or horizontal discontinuities. The vertical one represents sub-vertical tension cracks, and in

addition, there are two conjugate families of extension fractures. All the fractures are simulated independently. Their position is generated following a Poisson random point process with a density that is different for every fracture family. The distribution of the length of the fractures follows a truncated power-law distribution, with an exponent that has been kept constant. The orientations follow a von Mises distribution for each fracture family. All the parameters of those statistical distributions are provided in Table 1. In total, 6257 fractures were generated, and the total accumulated fracture network length is 57,627.83 m.

In numerous geological environments, it has been shown that fracture apertures are variable in space. Their apertures are spatially correlated at multiple scales (Tatone and Grasselli 2012). To generate a simple but plausible initial distribution of fracture aperture, we modeled it using a random multi-Gaussian field. The method is described in detail in Chilès and Delfiner (2009). The generation of the apertures is conducted in two steps. First, we simulated a correlated random multi-Gaussian field  $Z(x, y)$  which has a Gaussian marginal distribution. The field is generated using the Sequential Gaussian Simulation (SGS) algorithm within the Ar2GEMS software. The parameters used for the simulation are: (i) a Gaussian variogram model with a range equal to 150 m in the horizontal direction and 50 m in the vertical direction, and (ii) a mean equal to 0 and a variance equal to 1. The resulting distribution of apertures for the 2000 m by 500 m model domain has a log-normal distribution with

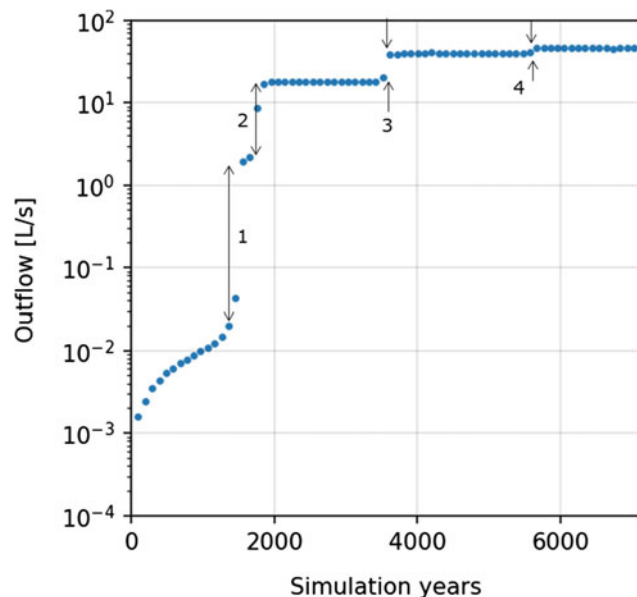
**Table 1** Input parameters to generate initial fracture network

Discontinuity family	Sub-horizontal fractures	Sub-vertical fractures	Conjugate fractures 1	Conjugate fractures 1
Min orientation [°]	88	-2	20	-40
Max orientation [°]	92	2	40	-20
Min length [m]	50	50	20	20
Max length [m]	500	300	300	300
Density	$2.5 \times 10^{-4}$	$2.5 \times 10^{-4}$	$1.4 \times 10^{-4}$	$1.4 \times 10^{-4}$

**Fig. 4** Hydraulic boundary conditions and initial fracture apertures

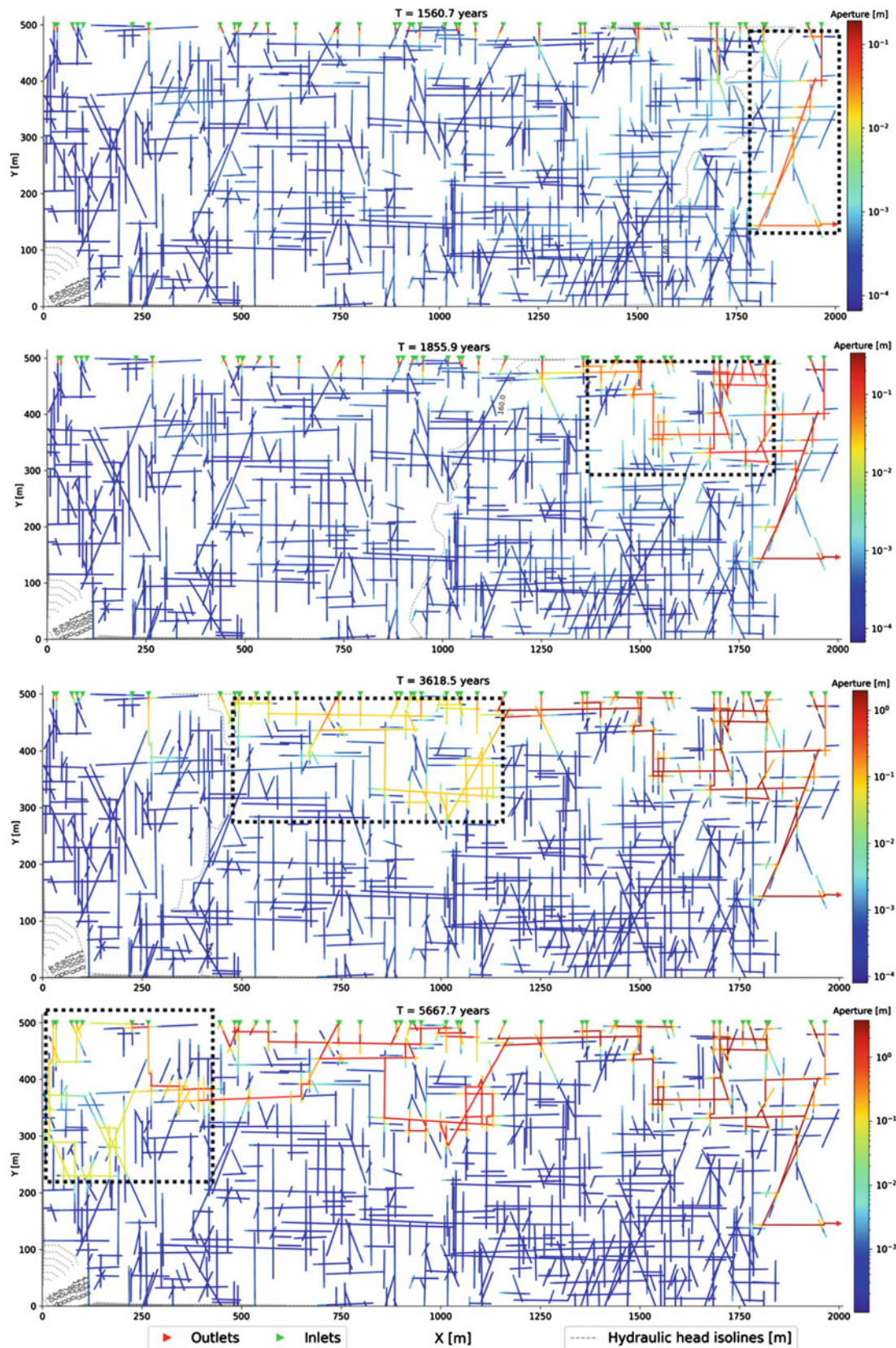
aperture values from  $5.0 \times 10^{-5}$  m to  $5.0 \times 10^{-4}$  m. Figure 4 presents the fracture network with the initial fracture aperture values. Fractures are discretized into smaller elements which have a unique aperture value. The hydraulic boundary conditions are 46 recharge nodes on the top model boundary and a single outlet node in the right boundary near the bottom. The hydraulic boundary condition is a constant hydraulic head of 33 m limited to a maximum flow rate of 1 l/s.

Figure 5 presents the evolution of flow rate before stabilization for scenario A, where we observe 4 sudden increases

**Fig. 5** Breakthrough times (1, 2, 3, 4) observed in flow rate evolution

in flow rates. Every increase in the outflow is related to a breakthrough of enlarged fractures connecting the inlet nodes with the outlet (see Fig. 6). The subnetwork of initial fractures that suddenly connects inlets and the outlet are identified and are highlighted with a dashed rectangle. Fracture growth in these regions caused sudden increases in the outflow rate. Increase 1 is the consequence of 1st breakthrough presented in Fig. 6 (top). Increase 2 in the outflow rate is caused by the second breakthrough (Fig. 6 second from top), and so on until the last increase in outflow rate caused by the 4th and final breakthrough as presented in Fig. 6 (bottom). At the outflow stabilization time, the sum of the length of fractures that transitioned to turbulent flow is 7730 m out of a total fracture length of 57,627 m (13%).

The breakthrough of enlarged fractures influences the fracture aperture distribution as shown on the histograms of fracture aperture (see Fig. 7). At time  $T = 0$  yrs., the fracture aperture has a log-normal distribution with a mode or peak 0 (histogram on the top left). At  $T = 1,560$  yrs., the 1st breakthrough causes an aperture mode (peak 1) of  $\sim 0.1$  m. At  $T = 1,855$  yrs., the 2nd breakthrough causes a 2nd aperture mode (peak 2) of  $\sim 0.1$  m. By then, the fractures of the 1st breakthrough have a new mode of  $\sim 0.3$  m (peak 1). At  $T = 3,618$  yrs., the third breakthrough causes another aperture mode (peak 3) of  $\sim 0.1$  m. At this time, peaks 1 and 2 of mode have merged into a single peak of  $\sim 1$  m. At  $T = 5,667$  yrs., the 4th and final breakthrough occur and yet another mode (peak 4) of  $\sim 0.2$  m emerges. By then, peaks 1, 2 and 3 have almost converged to an aperture between 1 and 3 m and can be regarded as karst conduits. At  $T = 5,667$  yrs., inflow rate stabilizes (see Fig. 5), and the simulation is



**Fig. 6** 1st (1,561 yrs.), 2nd (1,857 yrs.), 3rd (3,618 yrs.), and 4th breakthrough (5,677 yrs.) and stabilization of flow rate to 1 l/s at every inlet fracture

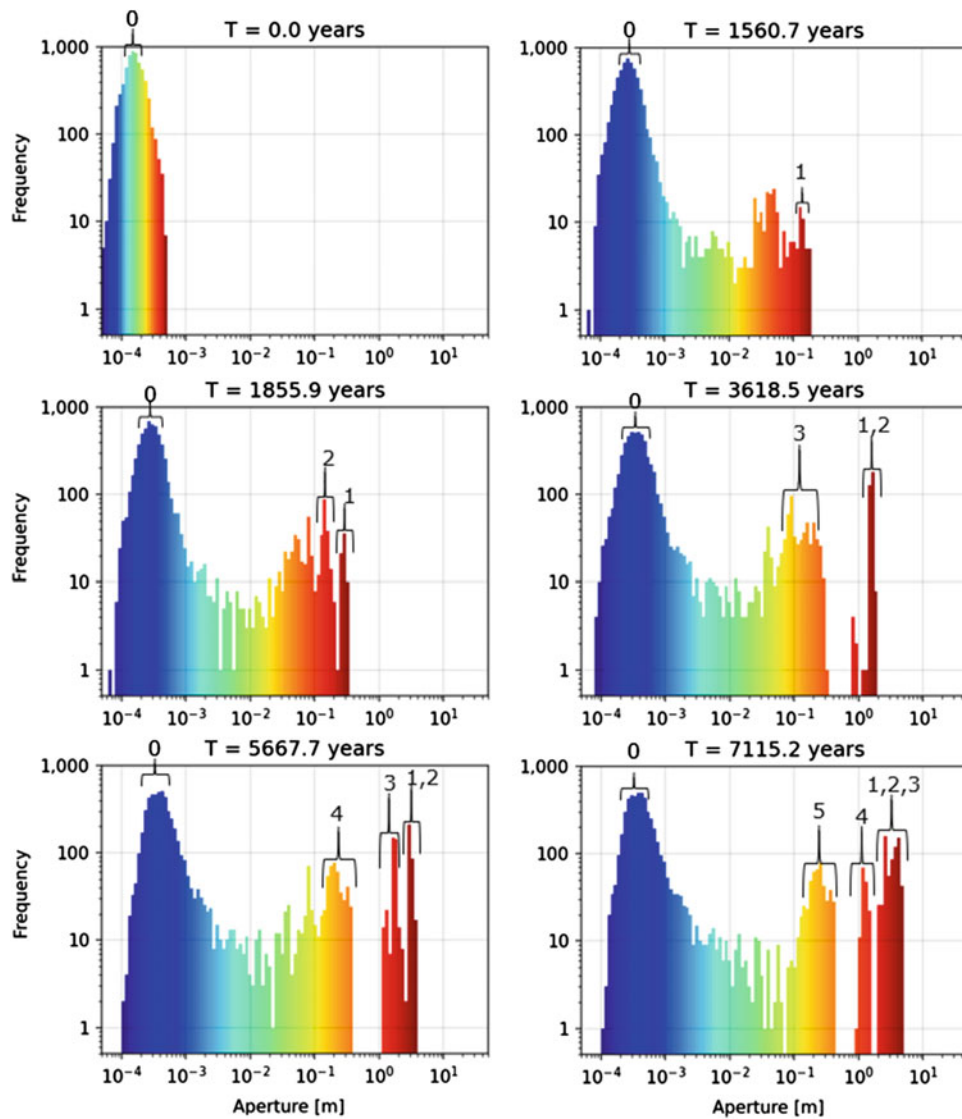


**Fig. 7** Histograms of fracture aperture at 1st, 2nd, 3rd, 4th breakthrough and final simulation time

left to run until  $T = 7,115$  yrs. At this evolution stage, the fractures of the 4th breakthrough (peak 4) almost converge with previous peaks 1, 2 and 3, and a 5th mode emerges with an aperture  $\sim 0.2$  m emerges. Since the inflow rate has stabilized, the flow in these fractures does not transition from laminar to turbulent flow and it is not expected that fractures of peak 5 grow into karst conduits.

## 5 Discussion and Conclusions

One striking feature of our results is that we observe and describe quantitatively that the karstification process does not occur homogeneously in a basin, but instead, it proceeds in a series of multiple breakthroughs corresponding to the different stages of karstification (Fig. 8) as it was proposed earlier by

Filipponi (2009). The original model included 3 phases in cave development: (i) inception, (ii) gestation and (iii) development. The inception phase is the start of dissolution in fractures under phreatic conditions. The outlet or spring is assumed to be the consequence of a valley incision in a soluble rock massif. The outlet organizes flow in the aquifer and at time 1 a cave gestation zone emerges. This is comparable to the initial conditions of our simulation. At time 2, breakthrough occurs, and the new karst conduit network acts as a spring for the upstream section of the model, which is comparable to the 1st breakthrough in our simulation. The karst conduits (cave development phase) offer less resistance to flow, thus the water table drops (hydraulic head in our simulation), and the gestation and inception zones move upstream. At time 3, the cave development keeps advancing upstream, which is comparable to the 2nd, 3rd and 4th breakthroughs in our simulation.

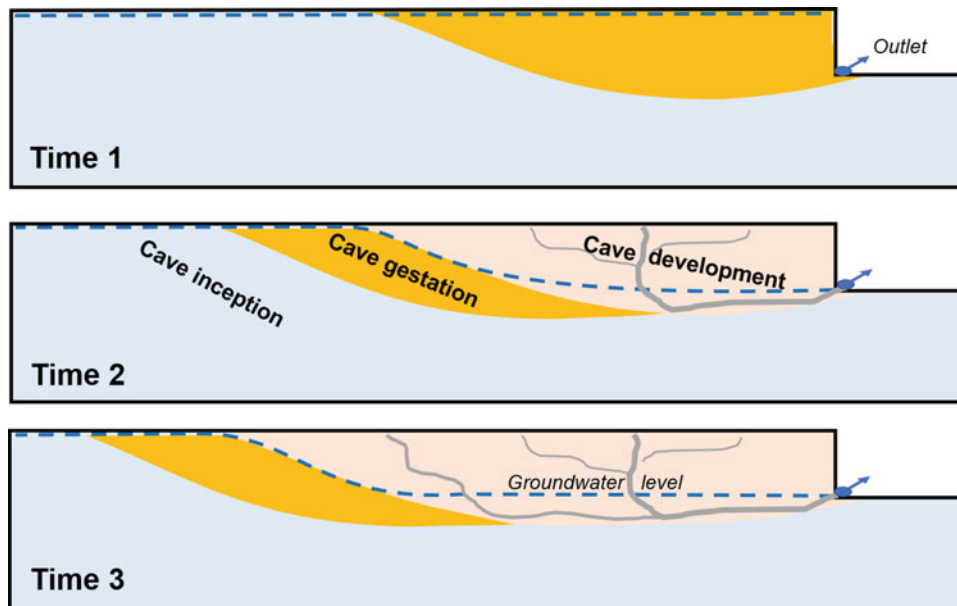


**Fig. 8** Conceptual model for the special development of karst conduit network

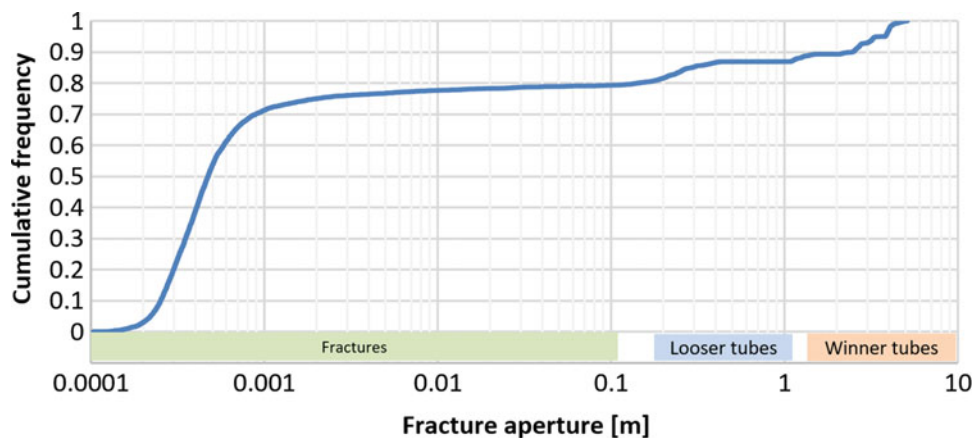


**Fig. 9** Cumulative fracture aperture at simulation time  $T = 7115$  yrs.

The growth process is heterogeneous, only 13% of the initial fracture length transitioned from laminar to turbulent flow. Fracture paths with greater resistance to flow stay at the initial size, and this is observed qualitatively in Fig. 6 and quantitatively in the histograms of Fig. 7. Figure 9 presents the cumulative frequency of fracture aperture at the end of the simulation. The distribution is trimodal with a first local maximum at undeveloped or slightly enlarged fractures smaller than 1 mm. A second mode at a size between 10 and 40 cm represents karst conduits that developed until the inflow rate stabilized. A third mode represents the karst conduits that continue growing while capturing most of the

inflow after flow rate stabilization. By observing the evolution of the geometry of the fracture network and the aperture distribution, we classify them as fractures, loser tubes and winner tubes.

Finally, an important result is the statistical distribution of conduit sizes. In this framework, we show that it tends to develop into a multimodal log-normal distribution even if the setup is very simple. The magnitude of the larger conduits, or winner tubes and their statistical distribution seems to be reasonable as compared to field observations in caves as presented in histograms of conduit size in Frantz et al. (2021) and Maqueda (2017).

## References

- Casagrande G, Cucchi F, Zini L (2005) Hazard connected to railway tunnel construction in karstic area: applied geomorphological and hydrogeological surveys. *Nat Hazards Earth Syst Sci* 5:243–250
- Chiles JP, Delfiner P (2009) *Geostatistics: modeling spatial uncertainty*. Wiley, New York
- Dreybrodt W, Gabrovšek F, Romanov D (2005) *Process of speleogenesis: a modelling approach*. ZRC Publishing, Postojna-Ljubljana
- Frantz Y, Collon P, Renard P, Viseur P (2021) Analysis and stochastic simulation of geometrical properties of conduits in karstic networks. *Geomorphology* 377
- Filipponi M (2009) Spatial analysis of karst conduit networks and determination of parameters controlling the speleogenesis along preferential lithostratigraphic horizons (Doctoral dissertation). EPFL, Laussane
- Filipponi M, Parriaux A, Schmassmann S, Jeannin P-Y (2012) KarstALEA: Wegleitung zur Prognose von karstspezifischen Gefahren im Untertagebau. *Forschung im Strassenwesen Bericht* 1395. UVEK, ASTRA, Bern
- Jeannin YP, Malard A, Rickerl D, Weber E (2015) Assessing karst hydraulic hazards in tunneling the Brunnmühle spring system Bernese Jura, Switzerland. *Environ Earth Sci* 74(12):7655–7670
- Maqueda A (2017) Process based modeling of the karstification processes in the region of Tulum, Mexico. PhD thesis. University of Neuchâtel, Switzerland
- Tatone BS, Grasselli G (2012) Quantitative measurements of fracture aperture and directional roughness from rock cores. *Rock Mech Rock Eng* 45(4):619–629